pH optimization for high-efficiency PEGylation of gold nanorods

Xingyu Du [1,2] · Wei-Chih Lin [2] · Qinghui Shou [1] · Xiangfeng Liang [1] · Huizhou Liu [1]

Abstract

The use of methoxy polyethylene glycol thiol (mPEG-SH), in conjunction with additives, is one of the most straightforward, versatile, and widely used methods for modifying gold nanorods (GNRs), especially for applications in the field of biomedicines. The decreased toxicity of PEGylated GNRs is critical for investigating cell-nanomaterial interactions. Most techniques suffer from low PEGylation efficiency. Several investigations of the PEGylation process have been conducted to determine its mechanism. Herein, we systematically investigated the qualitative and quantitative effects of the pH value on GNR PEGylation efficiency. The PEGylation process was applied to modify the GNRs at pH 0.3–14. PEGylation of GNRs at pH 2.3 and 9.9 resulted in better modification efficiency than under other pH conditions, achieving average PEGylation efficiencies of 95.5% and 83.6%, respectively. In both cases, the resulting GNRs could survive centrifugation after surface modification as demonstrated by measuring their longitudinal surface plasmon resonance (LSPR) UV-Vis absorption peaks. The aggregation index correlated to the PEGylation efficiency at the various pH levels. The origin of the differences observed at different pH values was also elucidated. These findings significantly expand the potential use of the aggregation index, as well as the understanding of processes used to modify gold nanoparticles.

Keywords Gold nanorods · Cetyltrimethylammonium bromide · PEGylation · pH value · Aggregation index

Introduction

Over the past two decades, GNRs have featured in promising applications in the fields of imaging [1], sensors, optics [2], anti-cancer agents, and LEDs [3]. Since GNR synthesis relies on the use of cetyltrimethylammonium bromide (CTAB), which exhibits significant cytotoxicity and colloidal instability, it is vital to modify the surface chemistry of the resulting GNRs to alleviate potential cytotoxicity, as well as to functionalize them for further applications [4, 5]. Among the various procedures for tuning GNR surface chemistry, thiol modification, which exploits the high affinity of sulfur for gold, is the most versatile method and can stabilize GNRs in a variety of solvents and improve their functionality through a relatively straightforward procedure [6].

Polyethylene glycol (PEG) is most commonly used for thiol modification. PEG is a neutral hydrophilic polymer that provides "stealth" character to nanostructures and imparts a high degree of stability and biocompatibility to GNRs [7, 8]. The standard GNR PEGylation protocol developed by Liao et al. involves one-step ligand exchange [9] by adding potassium carbonate and mPEG-SH directly to the GNR solution. Other PEGylation protocols (see Supplementary Materials Table S1) have also been reported. However, these methods still suffer from inadequate PEGylation efficiency, and high-yield ligand exchange with complete CTAB removal remains a major challenge [6, 8, 10, 11].

PEGylation is a complicated and multidisciplinary process involving various physical and chemical reactions. PEGylation requires several reaction steps, namely, the dissociation of the CTAB ligands, the diffusion of the PEG ligands into the CTAB layer, and the reaction or absorption of PEG-

✉ Wei-Chih Lin
   wc.lin@mail.nsysu.edu.tw

✉ Qinghui Shou
   shouqh@qibebt.ac.cn

1   CAS Key Laboratory of Bio-Based Materials, Qingdao Institute of Bioenergy and Bioprocess Technology, Chinese Academy of Sciences, Qingdao 266101, Shandong, China

2   Department of Mechanical and Electro-Mechanical Engineering, National Sun Yat-sen University, Kaohsiung, Taiwan

SH with gold [12]. During each step, the synthesis parameters and microenvironment must be precisely controlled to prevent certain problems, such as irreversible aggregation of the GNRs, from occurring. Several key factors that can affect the thickness, grafting density, and exchange efficiency of GNR PEGylation have been identified. For example, the removal of the CTAB coating by adding N,N-dimethylformamide (DMF) frequently results in the immediate aggregation of the gold nanorods [13]. After CTAB removal, PEGylation begins, and the PEG layer induces steric repulsion and van der Waals forces among the GNRs. The kinetics of the PEGylation mechanisms of the GNRs were clarified theoretically using the density functional theory (DFT) simulation approach [12]. From the experimental data, the team identified that the CTAB-PEG exchange reaction was a diffusion-limited process. Furthermore, researchers applied a method in which long-alkyl-chains were used as spacers between the PEG and thiol moieties to improve the grafting density of the coating [14]. Yuan et al. experimentally determined the role of the PEG-SH during the PEGylation process [15]. The added PEG initially caused coagulation of the GNRs, followed by their transformation from a coagulated to a dispersed state. The coagulation may be due to interaction between the gold surface and ether groups. However, the role of the thiol group during the PEGylation procedure has not been clarified. For further research and applications, this is a critical issue which deserves further intensive study.

Previous studies have investigated the influence of the pH value during PEGylation. In the standard PEGylation protocol reported by Liao et al. and developed by other researchers, potassium carbonate is generally added under alkaline conditions [9, 16–18]. Conversely, some researchers have utilized acidic conditions with a pH of ~ 3.0 to modify GNRs [19, 20]. Until now, only few pH conditions have been investigated. Thus, there is a need for systematic experimental studies to determine the modification mechanism. We expect that two key factors, the steric forces induced by the PEG molecule [21–23] and gold-thiol reactivity [24], might play vital roles in the efficiency of PEGylation. The present study thoroughly analyzed the effect of the pH on GNR PEGylation. GNRs and PEG-SH with a molecular weight of 5000 Da were mixed, and the pH was adjusted with HCl or KOH. After the PEGylation, transmission electron microscopy (TEM), X-ray photoelectron spectroscopy (XPS), zeta potential measurements, and nuclear magnetic resonance spectroscopy (NMR) were applied to characterize the PEGylated GNRs. To evaluate the effect of the surface chemistry of the GNRs on their aggregation behavior, GNR colloidal suspensions were studied using both the aggregation index (AI) and full width at half maximum (FWHM) parameters. These findings indicated that pH tuning can achieve a PEGylation efficiency of up to 95.5% PEGylation at pH 2.3.

Materials and methods

GNR synthesis and preparation of PEGylated GNR solutions

The seed-mediated method reported by Khanal et al. [25] was utilized to synthesize the GNRs in this research. We repeated their synthesis protocol and began the process by preparing the seed and growth solutions. Five milliliters of 0.2 M hexadecyltrimethylammonium bromide (CTAB, 99%, Sigma-Aldrich, Taiwan), 5 mL of 0.0005 M gold(III) chloride trihydrate (HAuCl$_4$·3H$_2$O, 99%, Alfa Aesar, Taiwan), and 0.6 mL of ice-cold 0.01 M sodium borohydride (NaBH$_4$, 98%, Sigma-Aldrich, Taiwan) were combined and stirred at 1200 rpm for 2 min. To prepare the growth solution, 250 mL of 0.2 M CTAB was added to 12.5 mL of 0.004 M AgNO$_3$ and 250 mL of 0.0010 M HAuCl$_4$·3H$_2$O. Then, 3.5 mL of 0.0788 M ascorbic acid (C$_6$H$_8$O$_6$, 99%, Sigma-Aldrich, Taiwan) was gently added and mixed with the prepared solution. Finally, 0.8 mL of the seed solution was slowly added to the prepared growth solution to synthesize the GNRs. The water used in all experiments was generated by an ultrapure water system (Rephile, Taiwan) and had a resistivity of 18.2 MΩ·cm at 25 °C.

The critical steps of GNR purification and excess CTAB removal were then undertaken. We achieved these two objectives using two centrifugation processes [26]. First, 250 mL of the synthesized GNR solution was centrifuged at 10,000 rpm for 40 min using a centrifuge (Hitachi, CR21GIII, Japan). The GNRs and excess CTAB could be separated, with the GNRs precipitating on the bottom of the centrifugation tube and the CTAB remaining suspended in the DI water. The GNRs were then suspended again in DI water. As demonstrated in a previous report, different geometries of synthesized gold nanomaterials, such as gold nanospheres and nanoparticles, can be separated by a low-speed centrifugation approach [27]. A centrifugation speed of 3000 rpm (1490×g for 10 min), which was calculated using the formula proposed in ref. [27], was utilized for collecting rod-shaped gold nanomaterials. After the low-speed centrifugation, the gold nanoparticles were concentrated at the bottom of the centrifugation tube, and the GNRs remained suspended in the supernatant. Finally, we collected the supernatant for use in subsequent experiments.

After the GNR purification and CTAB removal processes, the next step was PEGylation of the GNRs by adding mPEG-SH (methoxy PEG Thiol, PDI < 1.08, purity > 95%, Nanocs Inc., USA) to exchange the CTAB capped on the surface of the GNRs. Several teams have attempted to PEGylate GNR using PEG with a molecular weight of 5000 Da; they reported that higher molecular weight PEG ligands were not conducive to a high CTAB/PEG exchange rate. Additionally, the use of PEG with a molecular weight between 2000 and 5000 Da has

several advantages for biomedical applications, such as low cytotoxicity and a high circulation time in blood [7, 28]. For these reasons, we also utilized low (5000 Da) molecular weight PEG for GNR PEGylation in this study. In the PEGylation process, the amount of mPEG-SH added is a key factor. Therefore, we applied inductively coupled plasma-mass spectrometry (ICP-MS, PE-SCIEX ELAN 6100 DRC, Canada) to confirm the concentrations of purified GNRs in the supernatant. The amount of PEG that would be required to achieve full PEGylation of the GNRs was then calculated. As presented in the supporting materials, 4 mM of PEG was calculated to be sufficient and was added to each GNR supernatant in order to achieve the complete modification the GNRs.

To study the effect of the pH on the quality of the PEGylation, namely, the thickness, conformation, and condition of the PEG coating, we added either hydrochloric acid (HCl, Sigma-Aldrich, Taiwan) or potassium hydroxide solution (KOH, Sigma-Aldrich, Taiwan) to adjust the pH values of the PEGylated GNR solutions to values between 0.3 and 14 after adding the mPEG-SH solution. First, 7 mL of the purified GNR solution and 1 mL of the 0.2 mM mPEG-SH solution were combined for the PEGylation of the GNRs. Immediately after, 2 mL of an HCl or KOH solution of the appropriate concentration (see Table S3) was added to adjust the pH of each sample to the desired value. We immediately measured the pH of the GNR PEGylation solutions using a pH meter (HORIBA F-71 pH meter, Japan). Finally, the solution was stirred for 24 h to allow for thorough PEGylation of the GNRs.

Characterization of the synthesized GNRs and PEGylated GNRs

UV-Vis-NIR spectrometry is frequently applied to qualitatively and quantitatively analyze ligand exchanges. Several groups have evaluated the exchange of CTAB with PEG during the PEGylation of GNRs [29]. The aggregation index (AI) and full width at half maximum (FWHM) are two parameters that are frequently utilized to extract information from the UV-Vis spectrum. Equation 1 presents the formula to calculate the AI, which is equal to the area under the absorption spectrum divided by the longitudinal surface plasmon resonance intensity [29]. This parameter is concentration-independent and focused on the broader longitudinal surface plasmon resonance (LSPR) behavior. A higher AI indicates a greater degree of aggregation.

$$\text{Aggregation Index} = \frac{\int_{600 \text{ nm}}^{900 \text{ nm}} \text{Absorbance}(x) dx}{\text{LSPR Intensity}} \quad (1)$$

The FWHM can be determined using Gaussian fitting in the software Origin. Since the longitudinal plasmon peak is highly sensitive to aggregation, the colloidal stability of the PEGylated GNR solution was studied using the LSPR peak.

We measured the absorption spectrum of the CTAB-capped GNRs and the PEGylated GNRs prior to centrifugation using a UV-Vis-NIR spectrometer (Hitachi U-4100, Japan) in the range of 400 to 1000 nm with 0.5 nm steps. The average AI and FWHM were calculated at 0.5 pH intervals.

TEM is a powerful tool that is frequently utilized to view objectives at the micro- and nanoscale levels. In this study, we utilized TEM (JEM-2100, JEOL, Japan) to study the morphology, thickness, and uniformity of the as-synthesized and PEG-ligand-capped GNRs. The first TEM measurement was performed to obtain the initial morphologies, dimensions, aspect ratios, and thicknesses of the as-synthesized CTAB-capped GNRs. To analyze the PEG-capped GNRs, we first applied one round of centrifugation at 10,000 rpm for 10 min to reduce the influence of excess PEG on the TEM measurements, and then, the pellet was resuspended in water. Next, 1 mL of purified GNR solution was centrifuged for 10 min, and approximately 10 μL of the resulting GNR solution was spread on a carbon-coated copper grid (FC200, EM Resolutions, United Kingdom). TEM photos of the synthesized GNRs were obtained and analyzed using the software ImageJ to calculate their average dimensions and aspect ratios.

Zeta potential measurement is an easy, simple, and reproducible tool to ascertain the surface charge of a material. According to previous reports, CTAB and PEG have zeta potentials of ~ 40 and ~ 0 mV, respectively [7]. Therefore, the replacement of CTAB by PEG could be easily followed by the decrease in the zeta potential from 40 to 0. The higher the efficiency of the GNR PEGylation was, the greater the shift of the zeta potential would be. Samples were prepared by centrifugation at 10,000 rpm for 10 min after the PEGylation process. Then, a Zeta Potential Analyzer (Malvern Instruments, UK) was applied to measure the efficiency of the replacement of CTAB by PEG.

PEG reacts with water molecules, which could significantly affect the pH value of the PEGylated GNR solution. NMR spectroscopy (JEOL ECZ-600R 600 MHz NMR, Japan) was also utilized to study the effect of the pH on the efficiency of the GNR PEGylation. ^{1}H NMR spectra of the PEGylated GNR solutions with pH values from 0.3 to 13 were obtained to confirm the excess CTAB and PEGylated GNRs; these results were complementary to those obtained using XPS (see below). The PEGylated GNRs were frozen in liquid nitrogen and then lyophilized using a freeze dryer (EYELA FDU-2110, Japan) in a 15-mL centrifuge tube at a temperature of -90.3 °C and a pressure of 13.9 Pa for 48 h. Next, the

lyophilized GNRs were dissolved in deuterium oxide (D_2O) for ^{1}H NMR analysis. From the NMR spectra, the relative contents of CTAB and PEG were determined using the multiplet at about 3.30 ppm and the singlet at about 3.71 ppm, respectively. The area ratio was defined as the integration of the peak at 3.71 ppm divided by that of the peak at 3.30 ppm. As shown in Fig. S3, the chemical shift of PEO does not change with pH. The pH effect on the spectrum of the PEG was not remarkable. The area ratio was higher at pH 2.3 and in a weakly alkaline environment than under other conditions, indicating that the absorption of PEG on the GNRs was relatively larger under these conditions.

XPS was used to provide detailed information regarding the ligand composition on the GNR surface. XPS analyses were performed using auger electron spectroscopy (JEOL JAMP-9500F, Japan) and a surface analysis instrument (ESCA PHI 5000 Versa Probe, Japan). The samples were prepared using two rounds of high-speed centrifugation at 10,000 rpm for 10 min to remove the excess PEG after PEGylation. Then, 0.1 mL of each solution was dropped onto a 5 mm × 5 mm silicon wafer, dried in an oven at 80 °C for around 12 h. All spectra were obtained from the "coffee-ring" region [30]. The narrow scan was carried out at 1.0 eV and 0.1 eV using the auger electron spectroscopy (JEOL JAMP-9500F) and Versa probe (ESCA PHI 5000, USA), respectively. High-resolution elemental analysis was performed on the O 1s, C 1s, N 1s, and S 2p regions using CasaXPS software. We used the C 1s peak at 285.0 eV to calibrate the binding energy. Linear background correction of the standard Gaussian–Lorentzian fit was applied to the peak position and area calculations. Equation (2) was used to calculate the PEGylation efficiency [30].

$$\eta = \frac{C_0 - C}{C_0} \times 100\% \qquad (2)$$

C_0 refers to the percentage of nitrogen atoms on the original GNRs (a value of 6.6% was used in our experiments), and C is the percentage of nitrogen atoms obtained from the XPS spectra [30]. The average values for each sample were calculated.

Results and discussion

Characterization of the CTAB-capped GNRs and PEGylated GNRs

Figure 1a shows a typical TEM image of the as-synthesized GNRs. As can be seen from the TEM image, almost exclusively rod-shaped gold nanoparticles remained after three centrifugations. This proved that the centrifugation speed based on the calculated centrifuge force could precisely separate the

GNRs [26]. The average length and diameter of the synthesized GNRs were 44.7 ± 6.0 and 18.1 ± 2.9 nm, respectively. The aspect ratio was approximately 2.47. The averaged dimensions were obtained from over 300 TEM images using the software ImageJ. As presented in Fig. 1b, two SPR peaks at 519 nm and 741 nm were observed in the UV-Vis-NIR spectra. The peaks at approximately 520 nm and 780 nm corresponded to the longitudinal and transverse (lateral) surface plasmon resonance of the GNRs [31].

The effective ligand exchange of CTAB-capped GNRs depends critically on the effective removal of free excess CTAB [8, 10]. We applied centrifugation processes to decrease the CTAB concentration in the GNR solution to about 0.8 mM and to remove other impurities. The gold concentration in the solution was 28.9 mg/L according to ICP-MS measurement. As presented in the supporting material (Fig. SI), the minimum sufficient PEG concentration required for GNRs PEGylation was 4.91×10^{-7} mol/L.

Moreover, the pH value plays an important role in the stability of GNRs. Many reports have demonstrated that CTAB-capped GNRs suspended in solutions at pH 5.5 [32], 6 [29], 7 [33], 8 [34, 35], and 12 [36] were unstable. The increased ion-pair formation between OH^- and CTA^+ ions could result in poor coverage of CTAB on the GNRs, leading to their reversible aggregation [37]. The removal of the CTAB bilayer at an appropriate pH could be achieved in a few minutes, but the PEGylation process might require a longer time. To confirm this prediction, hydrogen chloride and potassium hydroxide solutions were used to adjust the pH values of the GNR suspensions, as shown in Fig. S1. With increasing pH, the localized surface plasmon resonance peak shifted and its intensity dropped, indicating that the stability of the GNRs decreased dramatically in the alkaline environment. A shoulder peak above 900 nm could be also observed. The aggregation of GNRs at pH values above 9 probably resulted from the disruption of the CTAB bilayer by the alkaline conditions [37]. Interestingly, the pH values of the GNR solution from 5.0 to 9.6 were unstable and fluctuating, which will be discussed later.

Study of the effect of pH on the efficiency of PEGylation

Several studies have demonstrated the use of the mPEG-SH ligand to replace the CTAB on GNRs. However, the mechanism of the ligand-exchange during the PEGylation process is very complicated and has not been addressed clearly. One report mentioned that efficient ligand exchange of CTAB-capped GNRs is critically dependent on the effective removal of free CTAB [13, 14]. This could be because the CTABs could reattach to the top surface of the mPEG-ligand, due to the high absorptivity of the CTAB. Therefore, centrifugation is a highly useful treatment to efficiently remove the excess CTAB. Conversely, the full elimination of CTAB from the

Fig. 1 **a** TEM image and **b** UV-Vis-NIR spectra of the CTAB-capped GNR solution

(a)

(b)
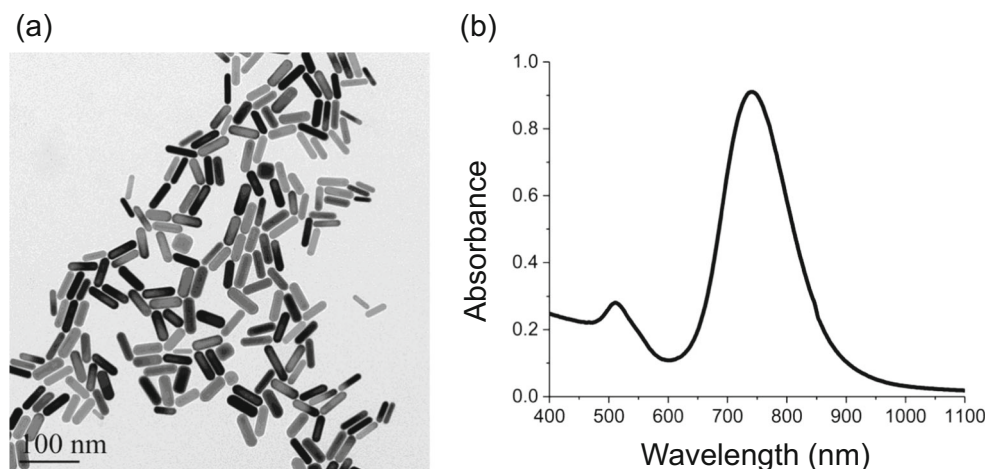
GNRs might result in the aggregation of the GNRs, which would result in a low mPEG-SH binding efficiency. The GNRs might aggregate due to the high attractive force of the metal-metal (gold-gold) bond. Therefore, appropriate removal of the CTABs is a critical step. We repeated the high-speed centrifugation process twice to remove excess CTAB to create an environment with a low concentration of CTAB for the PEGylation of the GNRs.

The CTAB-capped GNR solution was centrifuged to decrease the CTAB concentration to ~ 0.8 mM, and the pH value of the resulting solution was about 4–5. This low pH may have resulted from a large concentration of L-ascorbic acid after the centrifugation protocol. UV-Vis-NIR spectrometry was applied to qualitatively and quantitatively study the degree of ligand exchange, which could be utilized to evaluate the removal efficiency of the attached CTAB ligands, after PEGylation. The AI and FWHM values were calculated from the measured UV-Vis-NIR spectra and are presented in the Supplementary Information.

Various studies have examined the stability of GNRs in different pH ranges. These studies have proven that the GNRs did not undergo any significant change or degradation in acidic environments [29, 36, 38]. One team also reported that GNRs capped with the neutral ligand PEG were stable over nearly the entire pH range during the modification process [39].

The relationship between the pH value and the AI and FWHM is presented in Table 1 and Fig. 2a–d. In an acidic environment, the AI decreased dramatically in the pH range from 0 to 2.3 and increased from pH 2.3 to 5.0. The FWHM results showed a similar tendency that of the AI plot.

Figure 2c, d presents the AI and FWHM of the PEGylated GNRs at pH values between 9.3 and 14.3. The AI and FWHM gradually increased as the pH value increased. Compared to the CTAB-capped GNRs, after three rounds of centrifugation, the AI value increased more gradually and smoothly when mPEG-SH was added [29]. The lowest AI and FWHM values

were observed when PEGylation was conducted at pH values of 9.3 and 11.3.

Figure 3a shows the longitudinal surface plasmon resonance (LSPR) peak of GNRs PEGylated at pH values of 0.3, 1.3, 2.3, 2.8, 3.3, 4.6, and 4.7. The absorbance of the LSPR peaks declined as the pH value was increased from 2.3 to 4.6. Decreasing the pH value from 2.3 to 0.3 also resulted in a decreasing trend. These phenomena indicated that the GNRs modified at pH 2.3 exhibited the highest PEGylation efficiency among those PEGylated in acidic conditions. The PEG layer helped to maintain the dispersion of the GNRs after centrifugation. As shown in Fig. 3c, another round of centrifugation was performed in order to examine changes in the dispersion. The intensity of the longitudinal surface plasmon resonance peak of the GNRs that were PEGylated at pH 2.3 was maintained, while those of the other GNRs showed a remarkable decline. These results indicate that GNRs that were modified at pH 2.3 showed higher PEGylation efficiency than those modified at pH 3.3. The PEG layer helped to maintain the GNR dispersion after centrifugation. Similarly, the UV-Vis spectra of the GNRs PEGylated at pH values of 9.4, 9.9, 10.7, 10.9, 12.3, and 14.1 are presented in Fig. 3b. The LSPR peaks of the GNRs PEGylated at 9.4–9.9 were higher than those corresponding to other conditions. After one round of centrifugation, the GNRs PEGylated at pH 9.9 remained stable, while strong aggregation occurred for those PEGylated at pH 13.1–14.1, as shown in Fig. 3d. Therefore, the PEGylation efficiency might be related to the colloidal stability.

The TEM images from Fig. 4a–h show GNRs PEGylated in acidic and alkaline environments, specifically, at pH values of 0.3, 1.3, 2.3, 3.3, 4.3, 7.0, 9.9, and 13.1. Images for other pH values can be seen in Fig. S2. As can be clearly seen from Fig. 4b, c, the PEGylated GNRs and the conditions of the capped PEG layer, such as the thickness and uniformity of the PEG, could be clearly observed. The GNRs PEGylated at 2.3 showed a mostly homogeneous PEG layer, although

Table 1 Comparison of the gold nanorods' stability and PEGylation efficiency at different pH values

pH	AI	FWHM (nm)	Nitrogen atomic percentage	Percentage of C–O peak
0.3	191.4 ± 9.4	307.3 ± 19.2	2.4 ± 0.3	14.9 ± 0.6
1.3	151.4 ± 8.5	162.3 ± 14.1	3.4 ± 0.2	18.6 ± 4.8
1.6	151.3 ± 4.6	166.6 ± 10.6	0.37 ± 0.5	24.9 ± 4.5
2.3	151.9 ± 7.0	158.6 ± 6.6	0.3 ± 0.4	20.3 ± 9.3
2.6	155.3 ± 8.5	178.3 ± 36.5	1.7 ± 0.1	25.3 ± 7.7
3.3	161.9 ± 11.3	189.9 ± 35.9	1.7 ± 1.2	12.2 ± 3.6
4.3	162.1 ± 12.3	191.2 ± 39.5	2.3 ± 1.3	18.9 ± 6.0
9.4	163.9 ± 2.0	186.8 ± 2.7	2.2 ± 0.2	16.5 ± 6.4
9.9	174.7 ± 6.8	208.1 ± 49.1	1.5 ± 0.8	17.5 ± 8.6
10.3	176.9 ± 6.0	224.6 ± 42.0	1.5 ± 0.6	23.0 ± 7.0
10.9	175.5 ± 14.1	226.0 ± 35.0	1.8 ± 1.2	9.9 ± 5.2
11.9	176.3 ± 8.3	228.0 ± 46.6	1.4 ± 0.9	9.5 ± 4.6
13.1	188.2 ± 23.8	232.3 ± 47.6	2.2 ± 1.1	4.7 ± 4.7

there was still significant inhomogeneity in the capping. The average thickness of the PEG layer was approximately 3.0 nm. In comparison, the PEGylated GNRs at 1.3 showed more inhomogeneous PEG capping, and it is difficult to identify any PEG layer on the GNRs for pH values of 0.3, 3.3, and

4.3. Determining the cause of the uneven distribution is complicated; it might result from the low diffusion rate of the PEG ligand [12] and the surface migration of bound PEG [40], as presented in our experimental results above. In a previously reported simulation, the diffusion properties of PEG ligands
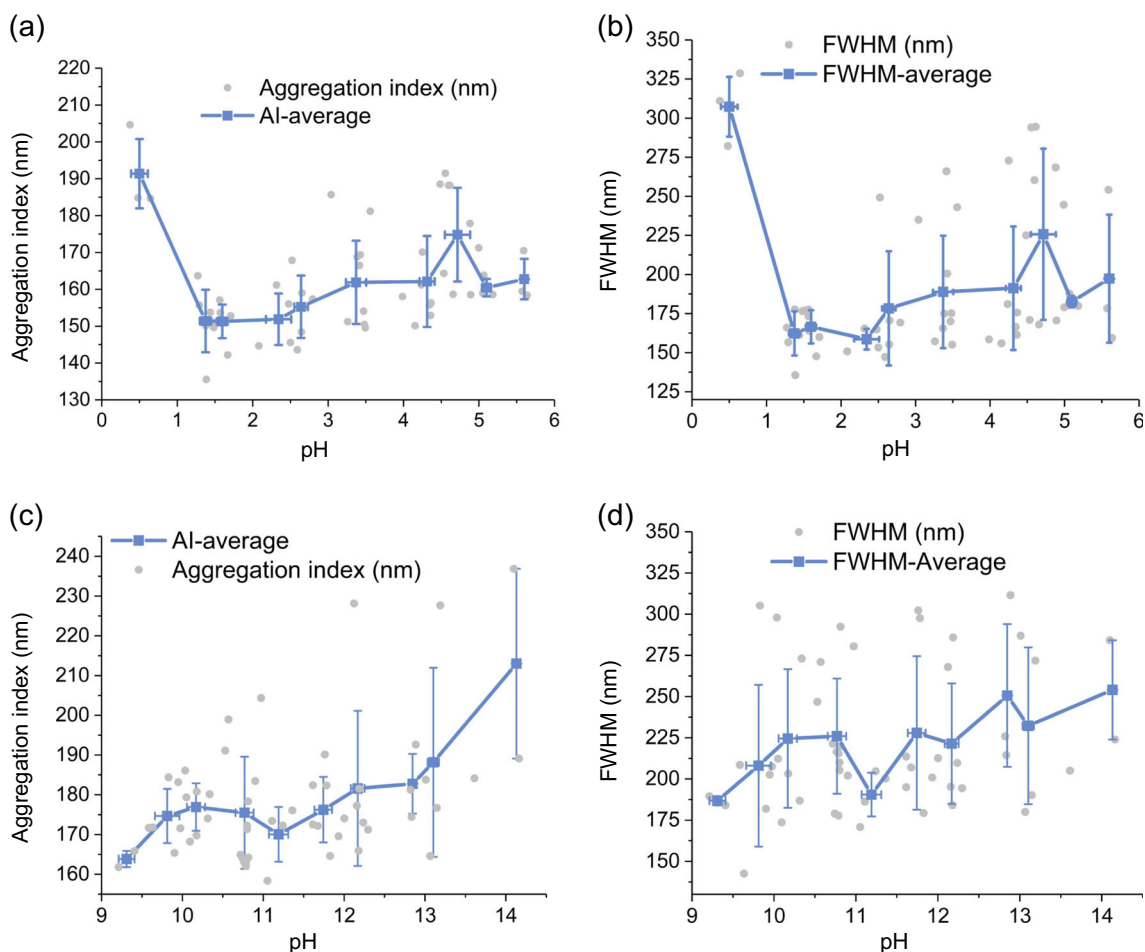
Fig. 2 **a**, **c** AI and **b**, **d** FWHM values at GNRs PEGylated at **a**, **b** acidic and **c**, **d** pH values
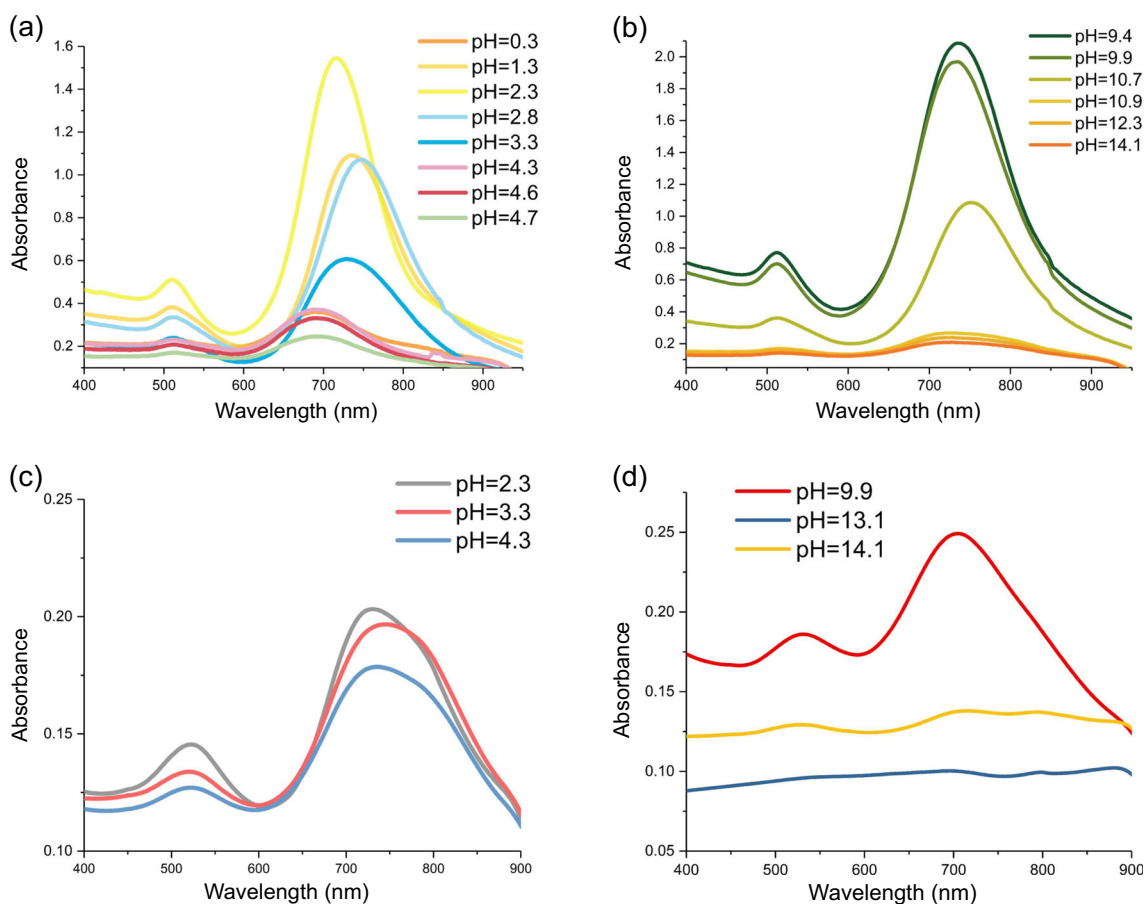
Fig. 3 Typical UV-Vis spectra of GNRs PEGylated in the pH ranges of **a** 0 to 5 and **b** 9 to 14 before centrifugation. UV-Vis spectra of GNRs PEGylated under **c** acidic and **d** alkaline conditions after centrifugation

were found to affect their absorption and exchange on gold nanoparticles [12]. On the other hand, the PEG attached on the GNRs surface could possibly freely migrate on the gold surface, similarly to in the place-exchange reaction on thiol protected gold nanoclusters [40]. Thus, the PEGylation

conducted at pH 2.3 could be favorable in terms of strongly disturbing the CTAB bilayer.

The pH value of the PEGylated GNR solution before adjustment was between 4 and 5. We adjusted the pH value by adding either HCl or KOH during the PEGylation procedure.
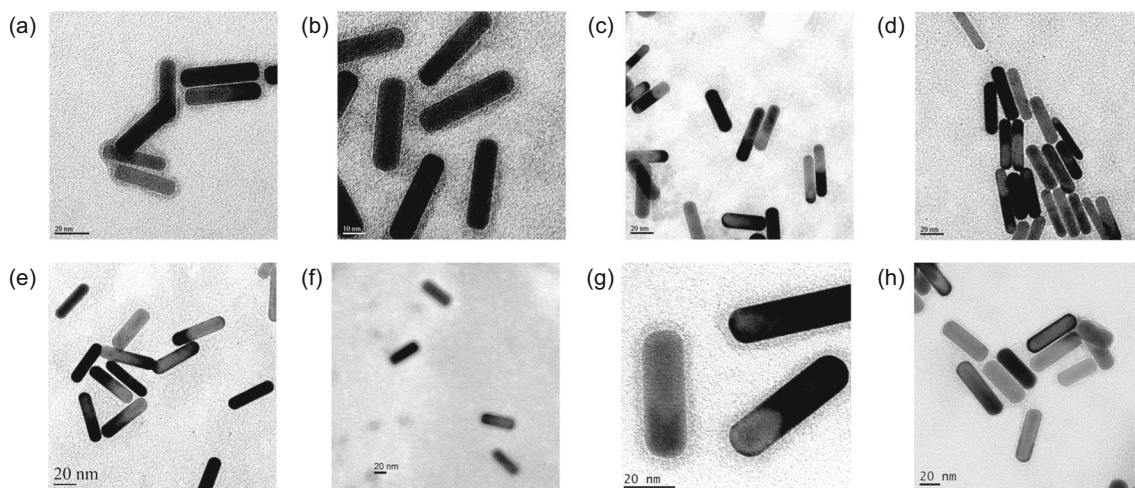

Fig. 4 GNR PEGylation in acid. TEM images of GNRs PEGylated at **a** pH = 0.3, **b** pH = 1.3, **c** pH = 2.3, **d** pH = 3.3, **e** pH = 4.3, **f** pH = 6.0, **g** pH = 9.9, **h** pH = 13.1 after negative staining

Figure 4f shows GNR PEGylated at a neutral pH using this approach. The entire surface of the GNRs was covered by PEG. Similarly, the PEGylation process was investigated under alkaline conditions at pH values between 9.1 and 13.1. As indicated in Fig. 4g, the homogenous modification of GNRs with PEG at was clearly observed at pH 9.9, and the average thickness of the PEG layer on the tail and shoulder was approximately 4 nm. In contrast, the GNRs PEGylated at pH 13.1 showed poor dispersion and inhomogeneous PEG modification, as shown in Fig. 4h. Therefore, the GNRs were functionalized with PEG in a weakly alkaline environment. Under strongly alkaline conditions, the PEG capping layers were nonuniform and difficult to identify.

Discussion

Assuming that the GNR solution consists of pure water and the added PEG, the ideal pH value can be calculated. As shown in Fig. 5a, the ideal pH values were similar to the actual values at pH < 5 and pH > 10. When the concentration of OH^- was 0.01 mM, the measured pH value was much lower than the ideal value. The electrical potential measurement of the pH meter did not stabilize within this range. The pure mPEG-SH showed the same trend (Fig. 5b). Williams et al. studied the ω-carboxylic acid-PEG-thiol passivated gold nanoparticles. A sharp change in the pH was observed upon the addition of KOH, which was due to the pKa of the carboxylic acid [41]. PEG is a hydrated polymer and is reported to have an ordered structure [42]. For aliphatic thiols, at higher pH values, covalent Au-S thiol linkages are more prevalent than Au-SH coordination [24]. For PEG-SH, the abrupt increase in pH may also relate to the thiol-gold reactivity. The pH change may become more remarkable when the pH is close to the pKa of the mPEG-SH.

The zeta potential of the GNRs was measured, and the results are shown in Table S6. The PEGylated GNRs had a positive zeta potential value in all cases, and all their potential values were lower those of the CTAB-capped GNRs. Although PEGylation could shield the capped CTAB layers and prevent the GNRs from aggregating, some CTAB still remained after modification. During the PEGylation of citrate-capped gold nanoparticles, PEG caused the coagulation of the gold nanoparticles, followed by their stabilization [15]. The coagulation force was attributed to the interaction of the PEG ether groups with gold. The GNRs in this study were also possibly anchored to PEG during the PEGylation process.

Figures 6a–d and 7a–d demonstrate the surface composition of the GNRs PEGylated in acidic and alkaline environments, respectively. The high-resolution elemental spectra of the PEG-capped GNRs, including the O 1s, C 1s, N 1s, and S 2p regions, was carried out; the resulting spectra are presented in Fig. 6a–d. Detailed information from the XPS measurements is reported in Table S3. The quantitative XPS results could be used to calculate the PEGylation efficiency on the surface of the GNRs. During the PEG and CTAB exchange process, the percentage of nitrogen atoms could be used to determine the percentage of CTAB removal, while the carbon and oxygen percentages could indicate the percentage modification with PEG. As can be clearly seen from Fig. 6a, b, the minimum and maximum nitrogen atom percentages and the carbon-oxygen peak ratios were observed at pH 2.3. Furthermore, the PEGylation efficiency and carbon-oxygen (C–O) peak reached approximately 95.5% and 20.28%, respectively. At pH 1.6, the PEGylation efficiency and C–O values were similar to those at pH 2.3. Therefore, we believe that the maximum PEGylation efficiency would be found between pH 1.3 and 2.3. Zhang et al. modified the techniques proposed by Liao [9] to demonstrate the high loading speed and coverage density of PEG on GNRs at pH 3. Similar results
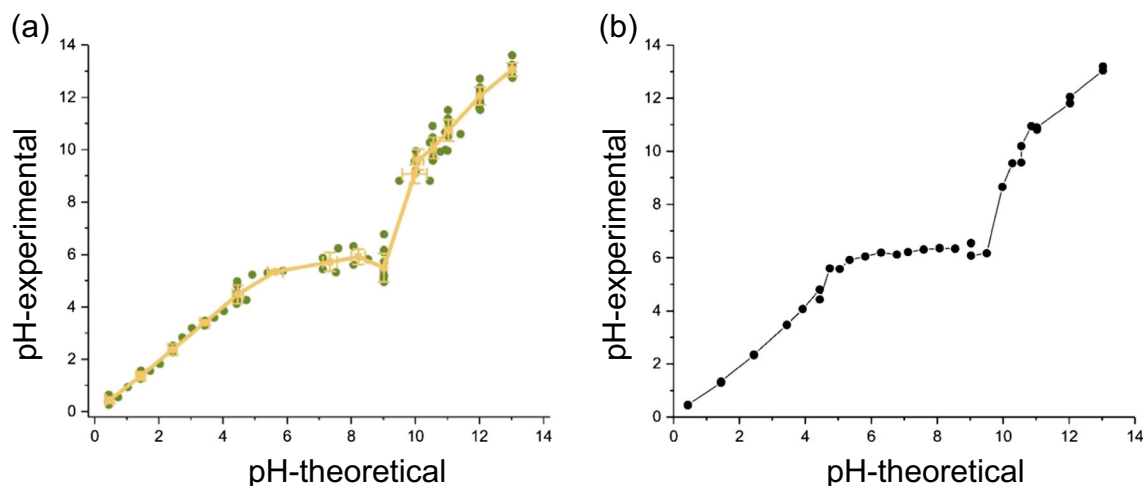

Fig. 5 Comparison of the ideal and actual pH values of the GNR solution after the addition of mPEG-SH (**a**). The pH change profile of pure mPEG-SH was also given (**b**)
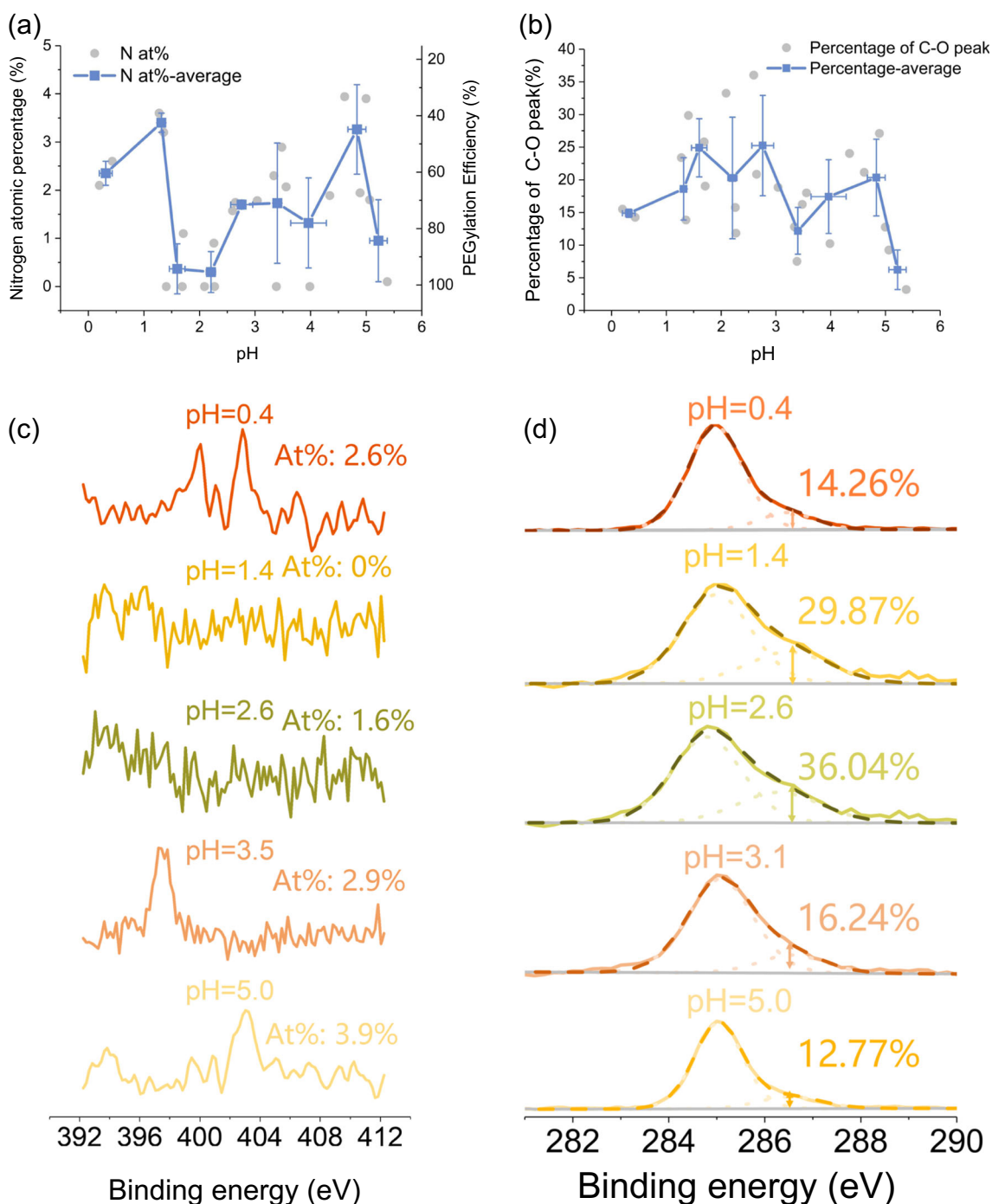
Fig. 6 GNRs PEGylated under acidic conditions. **a** Percentage of nitrogen atoms and PEGylation efficiency and **b** percentage of carbon and oxygen atoms at different pH values, as calculated from the XPS spectra. **c**, **d** Typical narrow scan results of **c** N 1s and **d** C 1s at different pH values

were also reported by Shi et al., who modified GNRs with thiolated DNA by adjusting the pH value to 3.0 [19].

Overall, the PEGylation process is strongly influenced by pH. At strongly acidic conditions such as pH 0.3, the GNRs can easily precipitate after centrifugation, which might be the cause of the low PEGylation efficiency. The absorption and desorption of PEG on silica nanoparticles has been investigated by Stuart et al. [43], who found that changing the pH could

change the protonation of the silica nanoparticles, thus affecting PEG absorption. In our case, the situation was more complicated since both the absorption and/or desorption behaviors of both CTAB and PEG were involved. An exploration of the exact details of the PEGylation process under acidic conditions is still in progress.

Under alkaline conditions, the highest PEGylation efficiency was observed in the weakly alkaline region between
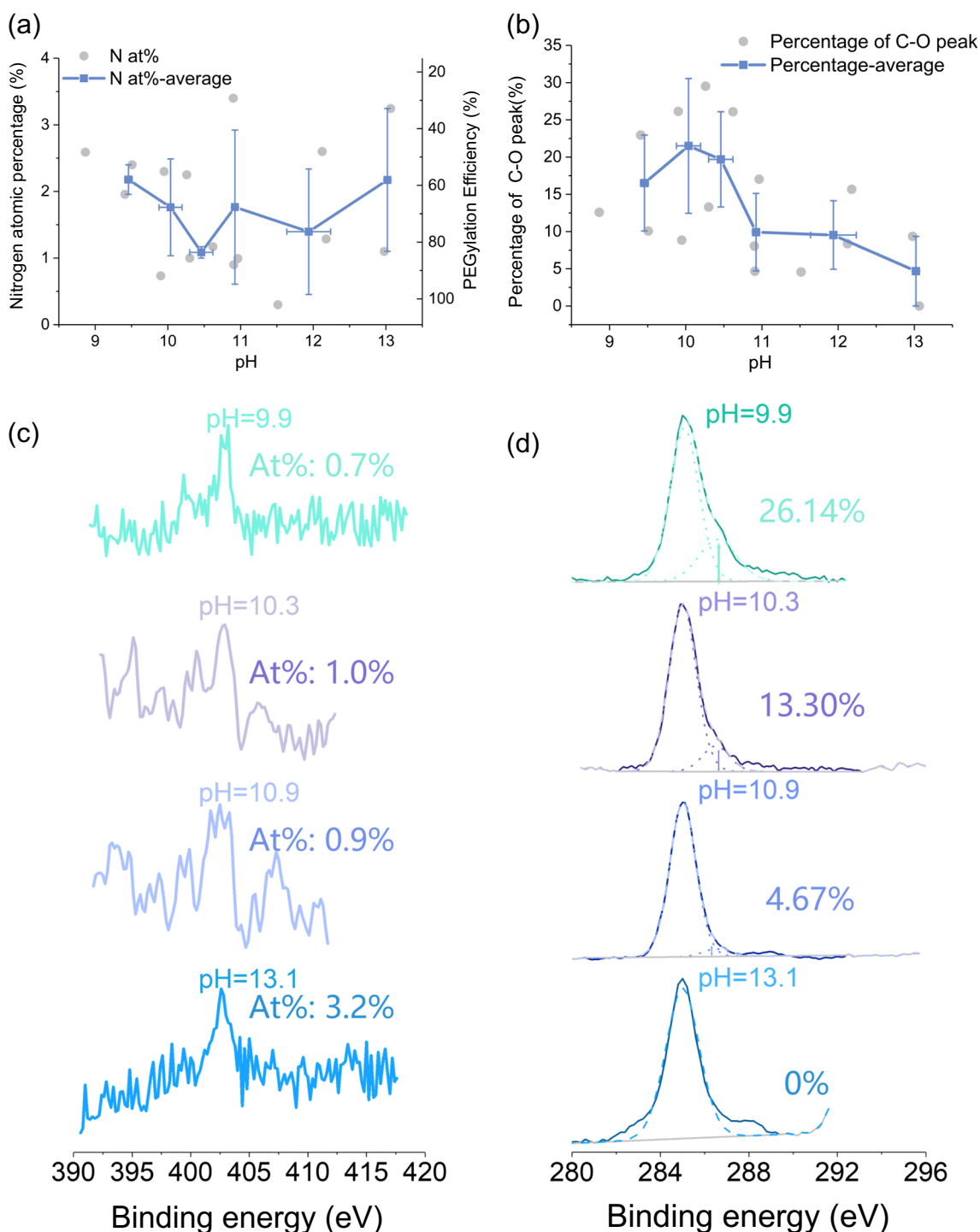
Fig. 7 GNR PEGylation in alkaline conditions. **a** Percentage of nitrogen atoms and PEGylation efficiency and **b** percentage of carbon and oxygen atoms at different pH values, as calculated from the XPS spectra. **c**, **d** Typical narrow scan results of **c** N 1s and **d** C 1s at different pH values

pH 9.9 and pH 10.3, as shown in Fig. 7a, b. A PEGylation efficiency of 83.6% and a C–O percentage of 19.7% were achieved at pH 10.3. Similarly, at pH 9.9, the PEGylation efficiency and C–O percentage reached 73.3% and 21.5%, respectively. The weakly alkaline environment range from about pH 8.5 to 10.3 may have assisted in breaking the S–H bond, which in turn might have increased the

PEGylation efficiency. Xue et al. employed atomic force microscopy-based single-molecule force spectroscopy to precisely assess the effect of pH on the mechanical strength of an isolated thiol-gold contact. They reported that an alkaline environment favored the dissociation of S–H, and that Au–S interactions became covalent at high pH [24]. Liopo et al. also reported that potassium carbonate

activates the SH group of mPEG-SH molecules [18]. It is worth noting that the pH value used by other reports with given amounts of potassium carbonate additive is in the range of 10.0~10.7 [16, 17, 44], the value of which almost correlates with our work.

Finally, the pH effect was studied using ^{1}H NMR. The area ratio was defined as the integration of the peak at 3.67 ppm, which corresponded to PEG, divided by the integration of the peak at 3.30 ppm, which corresponded to CTAB. As shown in Figs. S3 and S4, the chemical shift of PEO did not change with the pH. The area ratio was higher at pH 2.3 and in the weakly alkaline range than in other conditions, indicating that a relatively greater amount of PEG was adsorbed on the GNRs.

Conclusions

In this study, we systematically analyzed the effect of pH on GNR aggregation and PEGylation efficiency to elucidate the one-step physical process that converted cetyltrimethylammonium bromide-capped gold nanorods (CTAB-capped GNRs) into polyethylene glycol-capped GNRs (PEG-capped GNRs). The mechanism of the PEGylation of the GNRs is complicated, and the efficiency of the PEGylation of the GNRs could be described in terms of the steric force and gold-thiol reactivity. Various studies have demonstrated the good PEGylation of GNRs, but normally, these PEGylation experiments were conducted under either alkaline or neutral environments. In this study, we first synthesized CATB-capped GNRs and then PEGylated the GNRs at pH values between 0.3 and 13.1. XPS, UV-Vis, and TEM results demonstrated that higher PEGylation efficiency and stability were observed at pH 2.3 and pH 9.9. Moreover, capping of the GNRs with inhomogeneous and homogeneous PEG layers was achieved at pH 2.3 and pH 9.9, respectively. PEGylation at extremely low pH values, such as pH 0.3, resulted a low PEGylation efficiency, which might be caused by low thiol-gold reactivity during the PEGylation. However, in a mildly acidic environment, such as at pH 2.3, the repulsive forces decreased, increasing the efficiency of the GNR PEGylation. Interestingly, PEGylation in an alkaline environment resulted in contradictory effects, namely, increased thiol bond breakage and inhibition of the induction of coagulation via PEGylation.

Compliance with ethical standards

References

1. Chen YW, Liu TY, Chen PJ, Chang PH, Chen SY (2016) A high-sensitivity and low-power Theranostic Nanosystem for cell SERS imaging and selectively Photothermal therapy using anti-EGFR-conjugated reduced graphene oxide/mesoporous silica/AuNPs Nanosheets. Small 12(11):1458–1468

2. Lin L, Hong-Lian G, Xiao-Lan Z, Lu H, Jia-Fang L, Lin G, Zhi-Yuan L (2012) Manipulation of gold nanorods with dual-optical tweezers for surface plasmon resonance control. Nanotechnology 23(21):215302

3. Wu X, Liu L, Deng Z, Nian L, Zhang W, Hu D, Xie Z, Mo Y, Ma Y (2015) Efficiency improvement in polymer light-emitting diodes by "far-field" effect of gold nanoparticles. Part Part Syst Charact 32(6):686–692

4. Alkilany AM, Nagaria PK, Hexel CR, Shaw TJ, Murphy CJ, Wyatt MD (2009) Cellular uptake and cytotoxicity of gold Nanorods: molecular origin of cytotoxicity and surface effects. Small 5(6):701–708

5. Alkilany AM, Murphy CJ (2010) Toxicity and cellular uptake of gold nanoparticles: what we have learned so far? J Nanopart Res 12(7):2313–2333

6. Burrows ND, Lin W, Hinman JG, Dennison JM, Vartanian AM, Abadeer NS, Grzincic EM, Jacob LM, Li J, Murphy CJ (2016) Surface chemistry of gold Nanorods. Langmuir 32(39):9905–9921

7. Niidome T, Yamagata M, Okamoto Y, Akiyama Y, Takahashi H, Kawano T, Katayama Y, Niidome Y (2006) PEG-modified gold nanorods with a stealth character for in vivo applications. J Control Release 114(3):343–347

8. Vigderman L, Khanal BP, Zubarev ER (2012) Functional gold nanorods: synthesis, self-assembly, and sensing applications. Adv Mater 24(36):4811–41, 5014

9. Liao HW, Hafner JH (2005) Gold Nanorod bioconjugates. Chem Mater 17(18):4636–4641

10. Indrasekara ASDS, Wadams RC, Fabris L (2014) Ligand exchange on gold Nanorods: going Back to the future. Part Part Syst Charact 31(8):819–838

11. Garcia I, Henriksen-Lacey M, Sanchez-Iglesias A, Grzelczak M, Penades S, Liz-Marzan LM (2015) Residual CTAB ligands as mass spectrometry labels to monitor cellular uptake of au Nanorods. J Phys Chem Lett 6(11):2003–2008

12. Gao HM, Liu H, Qian HJ, Jiao GS, Lu ZY (2018) Multiscale simulations of ligand adsorption and exchange on gold nanoparticles. PCCP 20(3):1381–1394

13. Kim DH, Wei A, Won YY (2012) Preparation of super-stable gold Nanorods via encapsulation into block copolymer micelles. ACS Appl Mater Interfaces 4(4):1872–1877

14. Schulz F, Friedrich W, Hoppe K, Vossmeyer T, Weller H, Lange H (2016) Effective PEGylation of gold nanorods. Nanoscale 8(13):7296–7308

15. Wang W, Wei QQ, Wang J, Wang BC, Zhang SH, Yuan Z (2013) Role of thiol-containing polyethylene glycol (thiol-PEG) in the modification process of gold nanoparticles (AuNPs): stabilizer or coagulant? J Colloid Interface Sci 404:223–229

16. Liopo AV, Conjusteau A, Oraevsky AA (2012) PEG-coated gold nanorod monoclonal antibody conjugates in preclinical research with optoacoustic tomography, photothermal therapy and sensing.

In: Proc. of SPIE, vol. 8223, 822344. https://doi.org/10.1117/12.910838

17. Wang CU, Arai Y, Kim I, Jang W, Lee S, Hafner JH, Jeoung E, Jung D, Kwon Y (2012) Surface-modified gold nanorods for specific cell targeting. J Korean Phys Soc 60(10):1700–1707

18. Liopo A, Derry PJ, Ermolinsky B, Su R, Conjusteau A, Ermilov S, Zubarev ER, Oraevsky A (2014) Controlled Bacteria - gold Nanorod interactions for enhancement of optoacoustic contrast. In: Proc. of SPIE, vol. 8943, 894368. https://doi.org/10.1117/12.2044628

19. Shi DW, Song C, Jiang Q, Wang ZG, Ding BQ (2013) A facile and efficient method to modify gold nanorods with thiolated DNA at a low pH value. Chem Commun 49(25):2533–2535

20. Zhang Z, Lin MS (2014) Fast loading of PEG-SH on CTAB-protected gold nanorods. RSC Adv 4(34):17760–17767

21. Huang H, Penn LS, Quirk RP, Cheong TH (2004) Effect of segmental adsorption on the tethering of end-functionalized polymer chains. Macromolecules 37(2):516–523

22. Stuart MAC, Tamai H (1988) Dynamics of adsorbed polymers .2. Thickness relaxation of poly(ethylene oxide) on glass as a function of segmental binding-energy. Langmuir 4(5):1184–1188

23. Stuart MAC, Tamai H (1988) Dynamics of adsorbed polymers .1. Thickness relaxation of poly(Vinylpyrrolidone) on glass. Macromolecules 21(6):1863–1866

24. Xue YR, Li X, Li HB, Zhang WK (2014) Quantifying thiol-gold interactions towards the efficient strength control. Nat Commun 5:4348

25. Khanal BP, Zubarev ER (2007) Rings of nanorods. Angew Chem Int Ed Eng 46(13):2195–2198

26. Sharma V, Park K, Srinivasarao M (2009) Shape separation of gold nanorods using centrifugation. Proc Natl Acad Sci U S A 106(13):4981–4985

27. Scaletti F, Kim CS, Messori L, Rotello VM (2014) Rapid purification of gold nanorods for biomedical applications. MethodsX 1:118–123

28. Perrault SD, Walkey C, Jennings T, Fischer HC, Chan WCW (2009) Mediating tumor targeting efficiency of nanoparticles through design. Nano Lett 9(5):1909–1915

29. Kah JCY, Zubieta A, Saavedra RA, Hamad-Schifferli K (2012) Stability of gold Nanorods passivated with amphiphilic ligands. Langmuir 28(24):8834–8844

30. Liu K, Zheng Y, Lu X, Thai T, Lee NA, Bach U, Gooding JJ (2015) Biocompatible gold Nanorods: one-step surface functionalization, highly colloidal stability, and low cytotoxicity. Langmuir 31(17):4973–4980

31. Tong WM, Walsh MJ, Mulvaney P, Etheridge J, Funston AM (2017) Control of symmetry breaking size and aspect ratio in gold Nanorods: underlying role of silver nitrate. J Phys Chem C 121(6):3549–3559

32. Zhan QQ, Qian J, Li X, He SL (2010) A study of mesoporous silica-encapsulated gold nanorods as enhanced light scattering probes for cancer cell imaging. Nanotechnology 21(5):055704

33. Sethi M, Joung G, Knecht MR (2009) Stability and electrostatic assembly of au Nanorods for use in biological assays. Langmuir 25(1):317–325

34. Das M, Mordoukhovski L, Kumacheva E (2008) Sequestering gold nanorods by polymer microgels. Adv Mater 20:2371–2375

35. Ding H, Yong K-T, Roy I, Pudavar HE, Law WC, Bergey EJ, Prasad PN (2007) Gold nanorods coated with multilayer polyelectrolyte as contrast agents for multimodal imaging. J Phys Chem C 111(34):12552–12557

36. Ray TR, Lettiere B, de Rutte J, Pennathur S (2015) Quantitative characterization of the colloidal stability of metallic nanoparticles using UV-vis absorbance spectroscopy. Langmuir 31(12):3577–3586

37. Tiwari N, Kalele S, Kulkarni SK (2007) Modulation of optical properties of gold nanorods on addition of KOH. Plasmonics 2(4):231–236

38. Gole A, Murphy CJ (2005) Biotin-streptavidin-induced aggregation of gold nanorods: tuning rod-rod orientation. Langmuir 21(23):10756–10762

39. Gao J, Huang X, Liu H, Zan F, Ren J (2012) Colloidal stability of gold nanoparticles modified with thiol compounds: bioconjugation and application in Cancer cell imaging. Langmuir 28(9):4464–4471

40. Hostetler MJ, Templeton AC, Murray RW (1999) Dynamics of place-exchange reactions on monolayer-protected gold cluster molecules. Langmuir 15(11):3782–3789

41. Latham AH, Williams ME (2006) Versatile routes toward functional, water-soluble nanoparticles via trifluoroethylester-PEG-thiol ligands. Langmuir 22(9):4319–4326

42. Clop EM, Perillo MA, Chattah AK (2012) H-1 and H-2 NMR spin-lattice relaxation probing water: PEG molecular dynamics in solution. J Phys Chem B 116(39):11953–11958

43. Vanderbeek GP, Stuart MAC, Cosgrove T (1991) Polymer adsorption and desorption studies via H-1-Nmr relaxation of the solvent. Langmuir 7(2):327–334

44. Li C, Wu C, Zheng J, Lai J, Zhang C, Zhao Y (2010) LSPR sensing of molecular biothiols based on noncoupled gold Nanorods. Langmuir 26(11):9130–9135